*2452–2463* *Nucleic Acids Research, 2005, Vol. 33, No. 8*
*doi:10.1093/nar/gki538*

# Cyclohexenyl nucleic acids: conformationally flexible oligonucleotides

**Koen Nauwelaerts, Eveline Lescrinier, Gert Sclep and Piet Herdewijn***

Rega Institute for Medical Research, Laboratory for Medicinal Chemistry, Minderbroedersstraat 10, B-3000 Leuven, Belgium

Received as resubmission February 11, 2005; Revised and Accepted April 10, 2005

## ABSTRACT

**Cyclohexenyl nucleic acid (CeNA) is a nucleic acid mimic, where the (deoxy)ribose sugar has been replaced by cyclohexenyl moieties. In order to study the conformation of cyclohexenyl nucleosides by NMR, the HexRot program was developed to calculate conformations from scalar coupling constants of cyclohexenyl compounds, analogous to the methods applied for (deoxy)ribose nucleosides. The conformational equilibria and the values of the thermodynamic parameters are very similar between a cyclohexenyl nucleoside [energy difference between $_2H^3$ (N-type) and $^2H_3$ (S-type) is 1.8 kJ/mol and equilibrium occurs via the eastern hemisphere with a barrier of 10.9 kJ/mol] and a natural ribose nucleoside (energy difference between N-type and S-type is 2 kJ/mol and equilibrium occurs via the eastern hemisphere with a barrier of 4–20 kJ/mol). The flexibility of the cyclohexenyl nucleoside was demonstrated by the fast equilibrium between two conformational states that was observed in a CeNA-U monomer, combined with the $_2H^3$ conformation of the cyclohexene moiety when incorporated into a Dickerson dodecamer and the $^2H_3$ conformation when incorporated in a d(5′-GCGT*GCG-3′)/d(5′-CGCACGC-3′) duplex, as determined by the NMR spectroscopy. This represents the first example of a synthetic nucleoside that adopts different conformations when incorporated in different double-stranded DNA sequences.**

## INTRODUCTION

Ribonucleic acids are the most versatile and intriguing natural polymers. RNA has a lot of different biological functions: it is a messenger to transfer genetic information, a catalyst at the ribosome level, a primer in DNA replication, it plays a key role in the processing of precursor mRNA during splicing and editing, and it assists in RNA processing events, in the replication of viral genomes and in the control of translation (1). This is possible because RNA, in contrast to DNA, has a broad structural and functional versatility: it folds in a variety of tertiary structures and can catalyze a broad range of reactions, of which phosphodiester cleavage and peptide formation are the best known types. This versatility is ascribed to the presence of the ribose moiety as sugar in the backbone of RNA. The increased catalytic potential of RNA versus DNA is due to the presence of the 2′-OH group and the flexibility of the sugar moiety. Investigations on synthetic nucleosides that can mimic the properties of RNA have, for a long time, been too much focused on the synthesis of conformationally restricted N-type nucleoside analogs. Considerations about the dynamics of ribonucleotide structures have led to the synthesis of cyclohexenyl nucleic acids (CeNAs) (Figure 1). Since cyclohexene is one of the basic structures often used as a scaffold in organic chemistry, molecular geometry and conformational characteristics of cyclohexene were extensively investigated using various experimental and theoretical methods (2–5). As a result of the strong torsional constraint introduced by the double bond in cyclohexene, the two unsaturated carbons can be considered as a single pseudoatom (2), so that cyclohexene becomes analogous to a five-membered ring system with two preferred conformational states. As determined by different methods, the unsubstituted cyclohexene ring possesses an unusual energy profile for ring interconversion, where the transition from one twist-boat conformation to another via a high-energy boat conformation does not cause changes in energy. The barrier for this process is 4.2–10.3 kcal/mol, which is comparable with the barrier in puckering of ribose nucleosides. Biochemical tests have shown CeNA to be serum stable oligonucleotides that activate RNase H and form stable duplexes with RNA and DNA (6–13). Although cyclohexenyl has no free 2′-OH function, it was designed as a more flexible system than other RNA mimics that have been synthesized in view of their potential antisense activity. The potential for conformational flexibility of a nucleoside can be judged according to its possibility to adopt different conformations in different

*To whom correspondence should be addressed. Tel: +32 16 337387; Fax: +32 16 337340; Email: Piet.Herdewijn@rega.kuleuven.ac.be

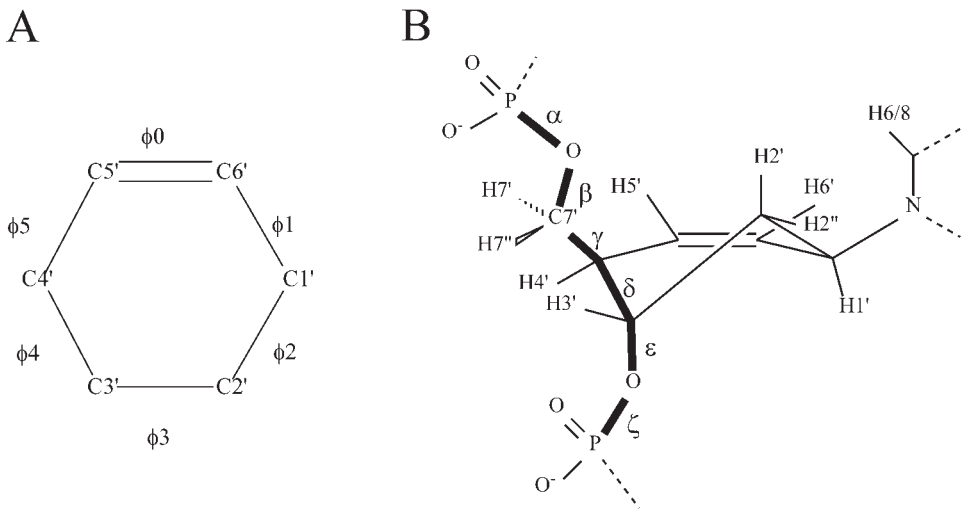


**Figure 1.** (**A**) Definition of endocyclic torsion angles and atom numbering in a cyclohexene ring and (**B**) definition of chemical structure, main torsion angles and atom numbering of a cyclohexenyl nucleoside incorporated in an oligonucleotide structure.

circumstances and to the energy profile involved in this conformational equilibrium. In this paper, we report results on changes in energy barrier and energy levels of the two favored conformations of a cyclohexene ring by the specific substituents in CeNA (1′-nucleobases, 3′-OH, 4′-$CH_2OH$ and 2′-OH); we describe puckering modes of the cylcohexene ring in terms of 'amplitude' and 'phase angle' analogous to natural RNA and DNA; we present a program that can be used to derive puckering parameters in a cyclohexene ring from measured NMR coupling constants; and finally, we demonstrate CeNA is the first example of a synthetic nucleoside that adopts different conformations when incorporated in different double-stranded DNA sequences. Such type of nucleoside analogs may have applications in biology, where the flexibility of the sugar moiety of the nucleoside is important for its function.

## MATERIALS AND METHODS

### Puckering parameters of cyclohexene ring

In five- and six-membered rings, the conformation of the ring can be described by puckering parameters (14,15). The conformation of a five-membered ring can be completely described by two independent puckering parameters: phase angle and puckering amplitude. Since the puckering amplitude stays within a narrow range and the pseudorotational angle can adopt values ranging from 0 to 360°, the different conformations are mostly visualized using the pseudorotational wheel (Figure 2) (14,16). Completely describing the puckering of a six-membered ring, however, requires three independent puckering parameters $Q$ (puckering amplitude), θ and φ (both phase angles) (15). Since $Q$ stays rather constant, θ varies from 0 to 180° and φ from 0 to 360°, the conformations can be represented on a conformational globe (Figure 2) (15).

The strong conformational constraint introduced by the double bond in cyclohexene keeps the two unsaturated carbons and atoms directly attached to them in one plane (2). This restriction in the motion of the cyclohexene ring limits the number of possible puckering modes and allows the elimination of one of the parameters necessary to describe an unrestrained six-membered ring. This was carried out using the truncated Fourier expansion method, which expresses the endocyclic torsion angles $\phi_j$, as defined in Figure 1, in terms of Fourier parameters: $\Phi_2$, $\Phi_3$ and $P_2$ (15).

$$\varphi_j = \Phi_2 \cdot \cos\left(P_2 + \frac{4 \cdot \pi \cdot j}{6}\right) + \Phi_3 \cdot \cos(\pi \cdot j) \quad \mathbf{1}$$

Since the unsaturated bond stays flat, $\phi_0$ can be regarded as 0°.

$$\varphi_0 = \Phi_2 \cdot \cos(P_2) + \Phi_3 = 0. \quad \mathbf{2}$$

$$\Phi_2 \cdot \cos(P_2) = -\Phi_3. \quad \mathbf{3}$$

When substituting Equation 3 into Equation 1, an equation is obtained that describes all endocyclic torsion angles of the cyclohexene ring with only two independent Fourier parameters $\Phi_2$ and $P_2$.

$$\varphi_j = \Phi_2 \cdot \cos\left(P_2 + \frac{4 \cdot \pi \cdot j}{6}\right) - \Phi_2 \cdot \cos(P_2) \cdot \cos(\pi \cdot j). \quad \mathbf{4}$$

To obtain analogy with the puckering amplitude and phase angle of pseudorotation as they are described in five-membered rings, we convert Fourier parameters $\Phi_2$ and $P_2$ into puckering parameters $Q$ and φ using Equations 5 and 6, which define the relation between Fourier and puckering parameters:

$$\varphi = P \quad \mathbf{5}$$

$$Q = \Phi_2 \cdot \sqrt{1 + \cos^2(P)}, \quad \mathbf{6}$$

where $Q$ can be considered as being the equivalent of the puckering amplitude and φ as the phase angle (15). In this manner, we can represent the different conformations of the cyclohexene ring on a pseudorotational wheel (Figure 3), similar to the one of the five-membered ring pucker.

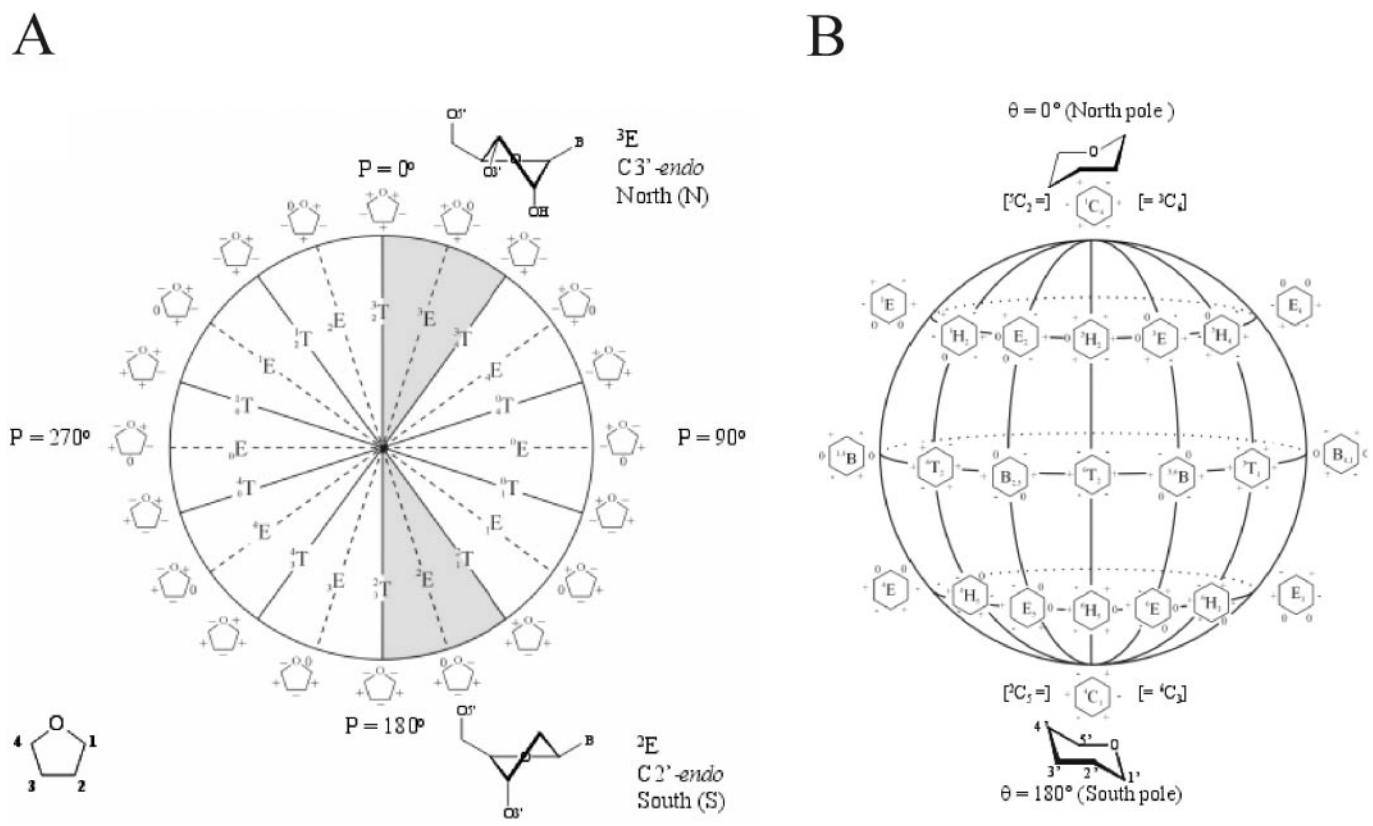


**Figure 2.** Conformations of five- and six-membered rings can be visually represented on the pseudorotational wheel (five-membered rings) and pseudorotational globe (six-membered rings).

### Calculation of potential energy surfaces of cyclohexenyl nucleosides

The potential energy surfaces of a thymidine cyclohexenyl nucleoside and its 2′-ribo-OH and 2′-ara-OH derivatives were calculated using computational methods. First, X-PLOR-NIH (17) was used to generate structures with specific φ and $Q$ values. Therefore, topallhdg.dna and parallhdg.dna files were adapted to include the modified residue using parameters reported in literature (18). Using restraints on the endocyclic torsion angles and restraining χ in the anti-domain, the starting structures with specific φ and $Q$ values were calculated. The energy of the obtained structures was subsequently optimized with MOPAC 6.0 (19) using the PM3 semi-empirical method (20,21). During this optimization, only endocyclic torsion angles were kept invariable permitting bond stretching and angle bending. A grid of different φ and $Q$ values was used with φ varying from 0 to 360° in steps of 3° and $Q$ varying from 28 to 56° in steps of 4°. In total, 840 grid points were used. The results were graphically represented on a polar plot and show that cyclohexenyl nucleosides have two low-energy states: $_2H^3$ (analogous to an N-puckered ribose) and a $^2H_3$ conformation (analogous to an S-puckered ribose). As a control, structures of 657 cyclohexenyl adenine, 724 cyclohexenyl guanine, 657 cyclohexenyl thymine and 724 cyclohexenyl cytosine nucleosides were randomly generated and energy minimized (22,23). Results are represented in Figure 3 and demonstrate that the spread between both the low-energy conformations in a CeNA monomer is independent of the nature of the nucleobase with all monomers having a preference for a $_2H^3$ conformation (A: 58%, T: 55%, C: 57% and G: 62%).

### Determination of five conformational parameters of cyclohexenyl nucleosides

Phase angle of pseudorotation (φ) and puckering amplitude ($Q$), which characterize the conformation of a cyclohexene ring, are related to endocyclic torsion angles (Equations 4–6) which in turn can be correlated to vicinal proton–proton coupling constants in the ring via the generalized Karplus equation (24–26) that has to be parameterized depending on electronegativities and position of substituents on the cyclohexene ring. Thus, for each cyclohexene conformation in CeNA, a set of $^3J_{H,H}$ can be calculated. Since theoretical calculations described above demonstrated that the cyclohexene ring in CeNA nucleosides occurs either in a $_2H^3$ or in a $^2H_3$ conformation, only $^3J_{H,H}$ of those conformations are relevant.

$$J_{\mathrm{calc1}}(Q1, \varphi 1) \quad \text{and} \quad J_{\mathrm{calc2}}(Q2, \varphi 2), \qquad \mathbf{7}$$

where $Q1$ and $Q2$ are puckering amplitudes in $_2H^3$ and $^2H_3$ conformation, respectively, and φ1 and φ2 are pseudorotation angles in $_2H^3$ and $^2H_3$ conformation, respectively.

If a rapid interconversion between two low-energy states exists, average J-couplings and chemical shifts are observed by NMR (27). This average depends on the relative abundance of both conformers.

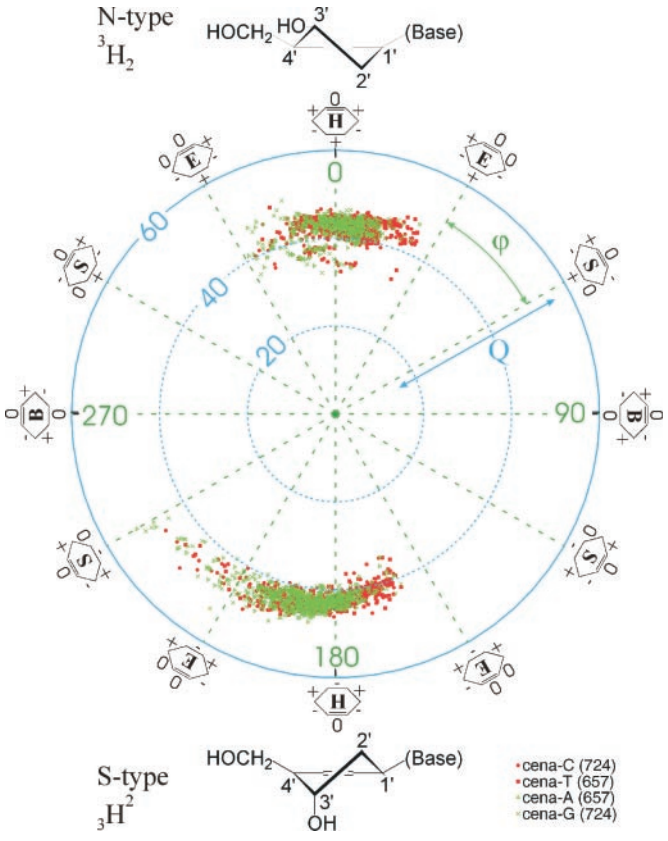


**Figure 3.** Pseudorotational wheel of a cyclohexene ring. Data points of 2775 structures that were random generated and energy minimized are represented. They show that the energetically most favorable conformations of the cyclohexene ring occur at the southern ($^2H_3$ or S-Type) or northern ($_2H^3$ or N-Type) poles of this wheel.

By introducing a new parameter describing the abundance of one of the conformers, the average $^3J_{H,H}$ coupling constants can be calculated:

$$J_{\text{calc}}^{\text{average}}(Q1, \varphi 1, f1, Q2, \varphi 2) = f1 \cdot J_{\text{calc1}}(Q1, \varphi 1) + (1-f1) \cdot J_{\text{calc2}}(Q2, \varphi 2), \quad \mathbf{8}$$

where $f1$ is the fraction of $_2H^3$ conformation in a two-state equilibrium.

## Development of the HexRot program

HexRot was developed to minimize the difference between the observed J-coupling constants ($J_{\text{obs}}$) and the average calculated coupling constants (Equation 8) by adjusting the five parameters defining the system ($Q1$, φ1, $f1$, $Q2$ and φ2).

The program was written entirely in Java® and apart from third-party libraries consists of a package encapsulating information about the observed coupling constants, core packages involved in the actual minimization, a package involved in parsing and writing out XML-like formatted input and output, a package containing the graphical user interface (GUI) classes and a package performing the communication between the core program layer and the GUI layer. The actual minimization was performed using a Quasi-Newton line search minimization routine. The latter was included in a Java port (http://www1.fpl.fs.fed.us/optimization.html) of the third-party unconstrained Newton/Quasi-Newton optimization package Uncmin and was slightly altered in order to allow for the definition of upper and lower boundaries for the input parameters. The JSci open-source library (http://www.sourceforge.net/projects/jsci) was used to plot the value of the minimized function along the axes of the used parameters. HexRot was designed to work with the Java® 2 Runtime Environment version 1.4.0 and the Java® 3D Application Program Interface version 1.3.1.

*Basic operation of the HexRot program*. Initially, one has to input the structure of the cyclohexene derivative, the observed coupling constants, as well as the parameters α and β describing the linear relationship between the endocyclic C–C–C–C torsion angles and the exocyclic H–C–C–H torsion angles of each measured coupling (28,29). This information can be given manually via a 3D or 2D interface or the information can be read from XML-like formatted input files (of which some examples are included with the program). For a subset of side chains, the program automatically derives the λ and ζ values (These parameters concern electronegativities and position of substituents and are used to parameterize the used Karplus equation.), used in calculating the coupling constants from the exocyclic H–C–C–H torsion angles (24–26). By allowing the λ values also to be entered manually, other side chains can be used as well. Prior to the actual minimization, initial estimates have to be given for the north and south phase angles of pseudorotation and puckering amplitudes as well as for the percentage of north conformation for each temperature at which the couplings were measured. If one opts to perform a constrained minimization, the preferred lower and upper bounds for each of these parameters have to be entered as well.

The plotted minimization function, shown after the completion of the minimization process, is useful when following the constrained optimization approach: if the curve intersects with the blue line, indicating the finally obtained minimization function value, one needs to broaden the allowed range of this parameter. Another provided means of gaining more insight into the quality of the performed minimization is the comparison of the calculated coupling constants and the experimentally derived coupling constants.

## NMR sample preparation

*Cyclohexenyl-U monomer*. After dissolution of 6 mg of the cyclohexenyl-U monomer in 0.25 ml $D_2O$, the pD was adjusted to 7.2. Afterwards, the sample was lyophilized and redissolved in 0.25 ml $D_2O$.

*d(5′-GCGT*GCG-3′)/d(5′-CGCACGC-3′) duplex*. The duplex used for the NMR experiments was obtained by titrating a DNA solution d(5′-CGCACGC-3′) with the complementary-modified sequence d(5′-GCGT*GCG-3′), in which T* represents a cyclohexenyl-T residue. The degree of complex formation was monitored by 1D NMR spectra of non-exchangeable base protons and anomeric protons. After titration, the pD of the sample was adjusted to 7.2. The sample was lyophilized and redissolved in 0.25 ml $D_2O$, resulting in a concentration of 2.8 mM of the duplex. The solution was

briefly heated to 80°C and slowly cooled to room temperature to promote duplex formation. For spectra in $H_2O$, the sample was again lyophilized and dissolved in 0.25 ml of 90%$H_2O$/10%$D_2O$.

### NMR spectroscopy

Spectra were recorded on a Varian Unity spectrometer (operating at 499.140 MHz). Unless stated otherwise spectra were recorded at 25°C. Quadrature detection was achieved in States–Haberkorn hypercomplex mode (30). Spectra were processed using the FELIX 97.00 software package (Accelrys©) running on a Silicon Graphics O2 R10000 workstation (IRIX version 6.3).

*Cyclohexenyl U monomer*. Scalar coupling constants between the cyclohexene ring protons were measured using 1D $^1$H NMR spectroscopy.

*d(5′-GCGT*GCG-3′)/d(5′-CGCACGC-3′) duplex*. The 1D spectra in $H_2O$ were recorded using a jump-return pulse as the observation pulse (31). The 2D NOESY in $H_2O$ (mixing time, 300 ms at 5°C) was recorded using the WATERGATE watersupression (32) with a sweep width of 10 000 Hz in both dimensions, 64 scans, 2048 data points in $t_2$ and 512 FIDs in $t_1$. The data were apodized with a shifted sine-bell square function in both dimensions and processed to a 2K × 1K matrix.

The 2D DQF-COSY (33), TOCSY (34) and NOESY (35) spectra in $D_2O$ were recorded with a sweep width of 4200 Hz in both dimensions. The residual HDO peak was suppressed by low power, on resonance, presaturation during 800 ms. The DQF-COSY spectrum consisted of 4096 data points in $t_2$ and 512 increments in $t_1$. The data were apodized with a shifted sine-bell square function in both dimensions and processed to a 4K × 1K matrix. Both $^{31}$P-decoupled (on resonance, continuous decoupling) and $^{31}$P-coupled spectra were recorded under the same conditions. For the TOCSY experiment, a clean MLEV17 (36) version was used, with a low power 90° pulse of 18.2 μs and the delay set to 47.3 μs. The total TOCSY mixing time was set to 50 ms. The spectrum was acquired with 32 scans, 2048 data points in $t_2$ and 512 FIDs in $t_1$. The data were apodized with a shifted sine-bell square function in both dimensions and processed to a 2K × 1K matrix. The NOESY experiments were acquired with mixing times of 50, 100, 150, 250 and 300 ms, 32 scans, 2048 data points in $t_2$ and 512 increments in $t_1$.

A $^1$H-$^{31}$P HETCOR (37) spectrum was acquired with 256 scans, 2048 data points in the proton dimension, $t_2$, and 256 increments in the phosphorus dimension, $t_1$, over sweep widths of 4200 and 1600 Hz, respectively. The data were apodized with a shifted sine-bell square function in both dimensions and processed to a 2K × 1K matrix.

### NMR-derived restraints of the d(5′-GCGT*GCG-3′)/d(5′-CGCACGC-3′) duplex

Distance restraints were derived from NOESY spectra recorded with 50, 100 and 150 ms mixing times, using the FELIX 97.00 software (Accelrys©). Based on the build-up curves, inter-proton distances were calculated. An experimental error (±20%) was used on the calculated inter-proton distances. The calibration of NOE cross peak intensities was carried out against the H5–H6 cross peaks as an internal standard and resulted in 58 intra-residue restraints and 107 inter-residues (6 of which are inter-strand).

Sugar puckers of the deoxyriboses in the DNA strand were inferred from the strong H1′ to H2′ (~9 Hz) and weak H3′ to H4′ (~2–3 Hz) scalar couplings, indicative of an S puckering of the sugar rings (38). Dihedral restraints on H1′–C1′–C2′–H2″ (157 ± 20°) and H2″–C2′–C3′–H3′ (−35 ± 20°) were used to constrain ribose conformation during the structure calculation; dihedral restraints on C1′–C2′–C3′–C4′ (−60 ± 40°) and C2′–C3′–C4′–C5′ (51 ± 40°) were used for the structure calculation to define the $^2H_3$ (S-Type) cyclohexene conformation based on the determined coupling constants and NOE effects as described in Results.

The β torsion angles of the duplex were restrained (to 180 ± 30°) based on the observable four bond $J_{H4'-P(n)}$ couplings (~4 Hz), indicating a W-shaped conformation of the atoms P–O5′–C5′–C4′ (38). The small and almost equal coupling constants (~3 Hz), which could be observed between P (T*4) and H7′/H7″ (T*4) (Figure 4), show the β torsion angle of the CeNA residue to be in a *trans* conformation (restrained to 180 ± 50°).

The small passive couplings observed in the H5′ to H5″ (DNA residues) cross peaks in the DQF-COSY spectrum and the nicely resolved H4′-P(*n*)-cross peak in the 2D $^1$H-detected [$^1$H,$^{31}$P] correlation spectrum allowed us to restrain the γ torsion angles in the DNA duplex to 60 ± 35° (38). In the cyclohexenyl-T residue, close NOE contacts were observed between H7′ and H4′, H7″ and H4′, H7″ and H3′, H7′ and H5′ (Figure 4). Analysis of proton distances in the different possible conformations around the γ torsion angle shows that this pattern of NOE contacts corresponds to a g+ conformation. The γ torsion angle of the CeNA residue was restrained to 60° ± 50°. The ε torsion angles of the DNA residues were restrained (to 230° ± 70°) based on steric arguments (39). In the CeNA residue, no ε torsion angle constraints were applied. The normal $^{31}$P chemical shifts of all regular DNA residues were used to restrain α and ζ torsion angles (0 ± 120°) (40). The ζ torsion angles of residue G3 and the α torsion angle of residue T*4 were not restrained since P (T*4) showed an irregular chemical phosphorus shift compared with the other phosphorous resonances (40).

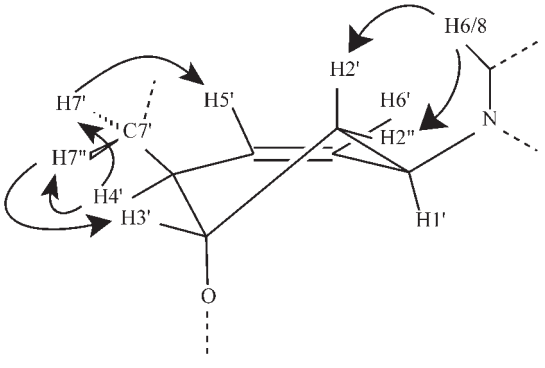


**Figure 4.** Important NOE contacts observed in the thymine cyclohexenyl residue (T*) in a DNA duplex consisting of d(5′-GCGT*GCG-3′) hybridized with d(5′-CGCACGC-3′).

### Structure determination of the d(5′-GCGT*GCG-3′)/ d(5′-CGCACGC-3′) duplex

All structure calculations were performed with X-PLOR-NIH (17). The topallhdg.dna and parallhdg.dna files were adapted to include the modified residue using parameters reported in literature (18). The CeNA residue was patched into the oligonucleotide sequence in a way comparable with the treatment of RNA and DNA in the standard X-PLOR program. The modeled structure of the CeNA monomer was used to derive energy constants.

The torsion angle molecular dynamics protocol used was largely identical to that proposed for a DNA duplex (41). A set of 100 structures was generated by torsion angle molecular dynamics, starting from two extended strands and using NMR-derived restraints.

After the torsion angle molecular dynamics round, the majority of the structures (70%) had converged to very similar structures with similar total energies (259–387 kcal/mol) and no violations of the NOE and dihedral restraints. The 25 lowest energy structures were used for further refinement during the 'gentle molecular dynamics' round.

The final refinement started with a 20 ps constant-temperature molecular dynamics simulation at 300 K (20 000 steps of 0.001 ps) and was followed by a 200-step conjugate gradient energy minimization of the average structure of the last 10 ps of the 20 ps simulation.

An analysis of the obtained 3D structure with the computer program X3DNA (42) was used to measure torsion angles and helix parameters. Finally, some visual representations of the molecule were obtained with Molscript 1.4 (43) and Bobscript 2.4 (44).

## RESULTS

### Calculation of potential energy surfaces of cyclohexenyl nucleosides

Our computational semi-empirical calculations on thymidine cyclohexenyl nucleoside and its 2′-ribo-OH and 2′-ara-OH show the existence of two important energy minima, corresponding to the $_2H^3$ (N-Type) and $^2H_3$ (S-Type) states and assess the quantity of the energy barrier between the two low energy wells (Figure 5). Furthermore, the results give us some indication of how the potential energy surface of the cyclohexenyl nucleosides can be tuned and modulated by choice of the substituents.

All calculated potential energy plots indicate that the lowest energy barrier between those two low energy states can be found in the eastern hemisphere of the pseudorotational wheel. The higher energy (compared with the eastern hemisphere), which was calculated in the western hemisphere, is probably caused by the close proximity of the base moiety and the C7′ group in this hemisphere. Both eastern and western structures show eclipsed conformations.

The energy plot of the deoxy cyclohexenyl nucleoside shows an energy difference between the $_2H^3$ (N-Type) and $^2H_3$ (S-Type) states of 1.8 kJ/mol with $_2H^3$ (N-Type) being the energetically most preferred conformation. This corresponds to the energy difference in a natural uracil ribonucleoside (2 kJ/mol) and a natural thymine ribonucleoside (2 kJ/mol) (45–47). The energy barrier of 10.9 kJ/mol between the two low energy states of deoxy cyclohexenyl thymidine is comparable with the barrier observed in potential energy studies of natural ribonucleosides and deoxyribonucleosides where energy barriers of 4–20 kJ/mol were observed (45).

If a 2′-OH function is substituted on the cyclohexenyl nucleoside in ribo position, a shift is observed from the $_2H^3$ (N-Type) to the $^2H_3$ (S-Type) state with $^2H_3$ (S-Type) becoming the energetically most preferred conformation. This shift can be explained by the 2′-OH and the nucleobase that occurs in an energetically favorable equatorial position (despite the fact that both other substituents are pseudo-axially oriented) and the gauche effect that exists between the nucleobase and 2′-OH and between the 2′-OH and 3′-OH when the molecule adopts the $^2H_3$ conformation. Furthermore, the transition barrier increases significantly from 10.9 to 17.5 kJ/mol, which can be explained by an eclipsed position of both hydroxyl groups in the eastern and western hemispheres.

The cyclohexenyl nucleoside derivative where the 2′-OH nucleoside is positioned in an arabino position was characterized by a larger energy difference between the $_2H^3$ and $^2H_3$ conformers (4.8 kJ/mol) with $_2H^3$ being the energetically most preferred conformation and an energy barrier comparable with the deoxy compound (8.1 kJ/mol). This behavior can be attributed to the stabilization of the $_2H^3$ state, where both hydroxyl groups occur in an equatorial position and are situated in gauche relative to each other and to the base moiety. In the eastern and western hemispheres, the OH-groups are not eclipsed and also occur in a gauche position relative to each other.

### Determination of conformational parameters of a cyclohexenyl nucleoside

In an NMR study of a uracil CeNA nucleoside, scalar coupling constants $^3J_{HH}$ were measured at different temperatures. The measured couplings do not correspond to the calculated coupling constants in either of the two low energy states, $^2H_3$ (S-Type) and $_2H^3$ (N-Type), determined in the computational approach mentioned above (Table 1). Since average, temperature-dependent $^3J_{HH}$ are observed, an equilibrium exists between the two states that is fast on the NMR time scale (27). Using the HexRot computer program, we analyzed the conformation of a uracil CeNA nucleoside at different temperatures and the corresponding equilibrium between $^2H_3$ (S-Type) and $_2H^3$ (N-Type) was calculated (Table 1). From these data, the $\Delta H$ and $\Delta S$ value of the equilibrium between the $^2H_3$ (S-Type) and $_2H^3$ (N-Type) was determined by means of standard Van't Hoff plots (Table 2). These results derived from NMR measurements give us an idea based on experimental data how large the energy differences between the $^2H_3$ (S-Type) and $_2H^3$ (N-Type) are. It is clear that the preferred conformational state of a uracil cyclohexenyl nucleoside at 27°C is the $_2H^3$ (N-Type) conformation, which is comparable with the energy calculations on a deoxy cyclohexenyl nucleoside mentioned before. Since gauche effects are absent in the ring under study, this phenomenon can be mainly attributed to the energetically favorable pseudo-equatorial position of the 3′-OH and 4′-$CH_2OH$ groups and to the $\pi$–$\sigma^*$ overlap within the allylic substituted heterocyclic system. It is obvious from the observed $\Delta S$ and

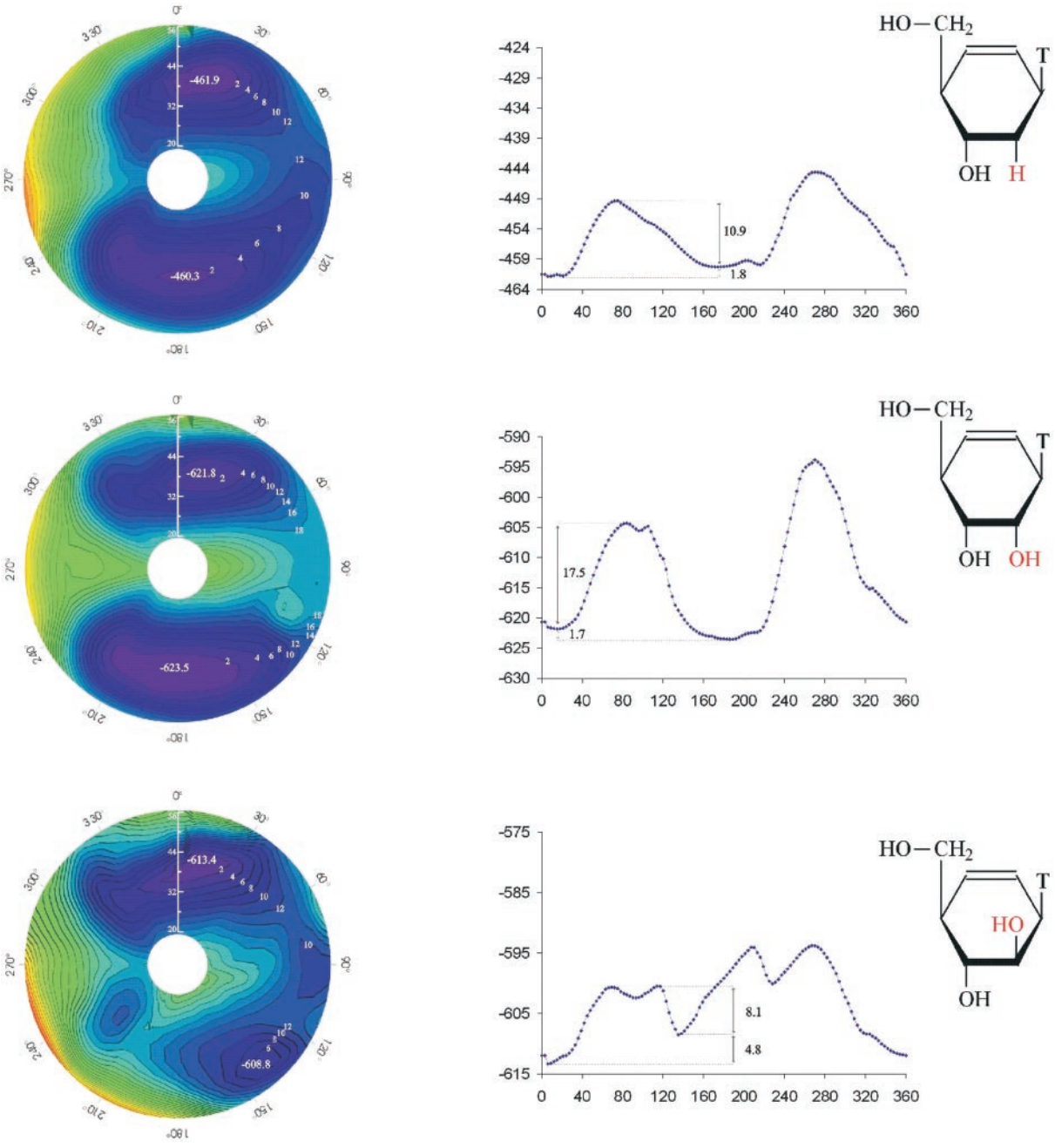


**Figure 5.** Potential energy plots of a cyclohexenyl nucleoside, a 2′-ribo-OH cyclohexenyl nucleoside and a 2′-ara-OH cyclohexenyl nucleoside.

$\Delta H$ values that enthalpy favors the $_2H^3$ (N-Type) conformation while the $^2H_3$ (S-Type) conformation seems to be preferred in terms of entropy. This gives good resemblance of the situation of a uracil ribonucleoside, where the conformational equilibrium is characterized by $\%N$ (27°C) = 53, $\Delta H$ = 2.0 kJ/mol, $\Delta S$ = 5.7 J/mol and $\Delta G$ (27°C) = 261 J/mol (48). It can be seen that the difference in $\Delta G$ between the uracil nucleoside and its cyclohexenyl equivalent is mainly due to the entropic contributions.

The measured coupling constants also give us an indirect indication of the energy barrier present between the two possible conformational states. Since average $^3J_{HH}$ are observed, the equilibrium between the two states can be regarded as fast on the NMR time scale. This poses an upper limit to the energy barrier between the two states.

### Structure determination by NMR spectroscopy of the d(5′-GCGT*GCG-3′)/d(5′-CGCACGC-3′) duplex

To investigate whether a cyclohexenyl nucleoside is able to adopt a $^2H_3$ (S-Type) conformation when incorporated in a DNA duplex despite its preference for a $_2H^3$ (N-Type) conformation as a monomer, a high resolution structure of a modified DNA duplex consisting of d(5′-GCGT*GCG-3′) hybridized with d(5′-CGCACGC-3′) was determined using NMR spectroscopy. The modification is represented by T*

and consists of a thymine cyclohexenyl nucleoside, inserted between residues G3 and G5. The atom numbering, chemical structure and main torsion angles of the modified part of the duplex are defined in Figure 1. This sequence was chosen because it allows us to study the behavior of one isolated cyclohexenyl nucleoside in a DNA duplex. In a former study, where a cyclohexenyl nucleoside (A*) was incorporated in a self-complementary DNA dodecamer with sequence d(5′-CGCGAA*TTCGCG-3′), a $_2H^3$ (N-Type) conformation of the cyclohexenyl nucleoside was observed and the incorporated nucleoside was found to influence the conformation of neighboring deoxyribonucleosides, shifting their conformations in the direction of the northern type (O4′-endo) (9).

**Table 1.** The conformation of a uracil CeNA nucleoside was measured using NMR spectroscopy

| $^3J_{H-H}$ (Hz) | 10°C | 20°C | 27°C | 40°C | 50°C | $_2H^3$ (N) | $^2H_3$ (S) |
|---|---|---|---|---|---|---|---|
| H4′–H3′ | 5.6 | 5.6 | 5.6 | 5.6 | 5.6 | 9.7 | 4.0 |
| H3′–H2″ | 8.2 | 8.2 | 8.1 | 8.1 | 8.1 | 11.6 | 2.7 |
| H3′–H2′ | 3.7 | 3.7 | 3.7 | 3.6 | 3.6 | 4.0 | 3.1 |
| H2″–H1′ | 5.9 | 5.9 | 5.9 | 5.9 | 5.9 | 1.6 | 11.1 |
| H2′–H1′ | 5.6 | 5.6 | 5.7 | 5.7 | 5.8 | 5.1 | 6.7 |
| % $_2H^3$ | 57.5 | 57.0 | 56.4 | 55.8 | 55.4 | 100 | 0 |

Scalar coupling constants $^3J_{HH}$ at different temperatures and the corresponding equilibrium between $^2H_3$ (S-Type) and $_2H^3$ (N-Type) are listed. Reference values for $^2H_3$ (S-Type) and $_2H^3$ (N-Type) puckered cyclohexenyl nucleosides were derived from $^2H_3$ (S-Type) and $_2H^3$ (N-Type) uracil CeNA nucleoside models, minimized by *ab initio* calculations.

**Table 2.** Conformational and thermodynamic parameters describing the equilibrium between $^2H_3$ (S-Type) and $_2H^3$ (N-Type)

| | $_2H^3$ (N-type) | $^2H_3$ (S-type) |
|---|---|---|
| φ | −20° | 202° |
| *Q* | 37° | 48° |
| $\Delta H$ ($_2H^3 \leftrightarrow {}^2H_3$) | 1.7 kJ/mol | |
| $\Delta S$ ($_2H^3 \leftrightarrow {}^2H_3$) | 3.5 J/mol | |
| $\Delta G$ ($_2H^3 \leftrightarrow {}^2H_3$) (27°C) | 660 J/mol | |

Non-exchangeable protons in the entire duplex could be assigned starting from a standard anomeric to aromatic proton walk (49). Sequential connectivities could be achieved (Figure 6) in the natural as well as in the modified portion of the duplex, and provided assignments for H1′ H5, H6 and H8 protons. The other protons of the spin systems were assigned from TOCSY, DQF-COSY and NOESY spectra (38). The $^{31}P$ resonances were assigned from the 2D $^1H$-detected [$^1H$,$^{31}P$] correlation spectrum (HETCOR). One-dimensional imino-proton spectra recorded at various temperatures in 90% $H_2O$/10% $D_2O$ showed five sharp signals between 12.5 and 14 p.p.m. The five sharp signals could be assigned via imino-H1′ and imino-to-adenine H2 cross peaks in the 2D WATERGATE-NOESY, which was confirmed by an imino-to-imino sequential proton walk (data not shown). Owing to fraying at the helix ends, imino signals of G1 and G7 could not be observed; resonance assignments in Supplementary Material.

An S puckering of the deoxyribose nucleosides and a $^2H_3$ conformation (equivalent of ribose S puckering) of the cyclohexenyl nucleoside were evident from various experimental observations. In the deoxyriboses, strong COSY peaks were observed from H1′ to H2′ and from H2′ to H3′. Analysis of the H3′–H4′ (T*4) and H4′–H7′ (T*4) COSY cross peaks with ACME (50) showed relatively small $J_{H2'-H3'}$ (∼3 Hz), $J_{H2''-H3'}$ (∼3.5 Hz) and $J_{H3'-H4'}$ (∼3.3 Hz) in the cyclohexene ring, resulting in a $^2H_3$ puckering (S-type) of the CeNA residue by HexRot (see Supplementary Material). Very strong NOE contacts between H2′ (T*4) and H6 (T*4) and between H2″ (T*4) and H6 (T*4) confirm these observations (Figure 4).

Various experimental results show the formation of a stable B-type helix in the modified and unmodified regions. The thermal stability of imino-protons is characteristic for stable base pairing in the central part of the duplex that includes the modified site. Typical NOE interactions of the base protons with a continuous aromatic to anomeric and aromatic to aromatic proton walk could be observed throughout the complete helix, including the modified part, and is indicative of

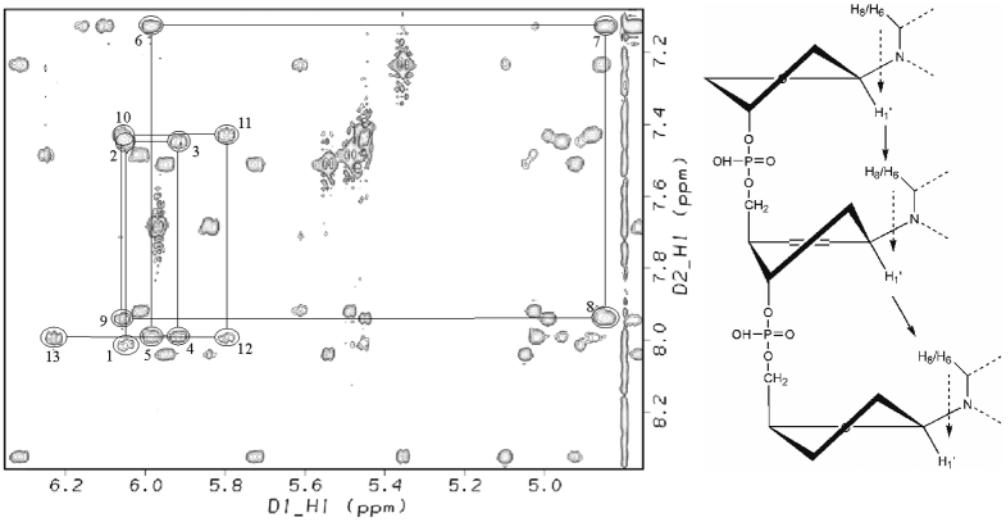


**Figure 6.** Anomeric to aromatic proton walk, used to assign the modified strand. H1′–H6/H8 cross peaks of the modified strand d(5′-GCGT*GCG-3′) are numbered. Intraresidue cross peaks: 1:G, 3:C, 5:G, 7:T*, 9:G, 11:C, 13:G.

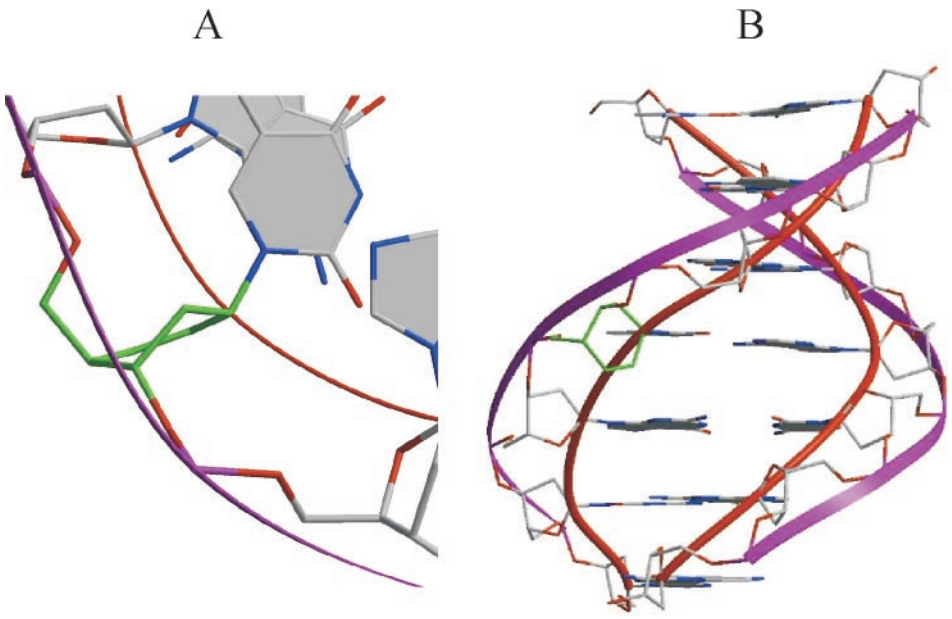


**Figure 7.** 3D representation of the structure determined by high resolution NMR spectroscopy. **(A)** Detailed view of the modified part of the duplex. It can be seen that the cyclohexenyl building block adopts a $^{2}H_{3}$ (S-Type) conformation. **(B)** Overall view of the duplex which shows to be B-type in the modified and unmodified regions.

regular base-stacking in a B-type helical structure. NMR spectroscopic information about the duplex backbone indicates a regular B-type conformation of the backbone in the unmodified region. This portion of the duplex shows strong couplings between P and H4′ of the previous residue and between P and H4′ of the next residue and all phosphorus resonances show regular chemical shifts. However, in the modified region, the T*4 phosphorus is strongly downfield shifted and no strong coupling could be observed between H4′ (T*4) and P (T*4), indicating an alternate conformation of the duplex backbone in the modified region. It might, however, be possible that due to the different structure of the cyclohexenyl nucleoside, this alternate backbone conformation is necessary to accommodate itself into a regular B-type helix.

To calculate the structure of the modified duplex, we performed torsion angle molecular dynamics (41) followed by a refinement of 25 selected structures using the NMR-derived restraints, as described in Materials and Methods. During calculation, the structures converged to a family of structures with similar geometry that fulfill all experimental restraints. Inspection of the obtained structures shows that the cyclohexenyl nucleoside occurs in a $^{2}H_{3}$ conformation (S-Type) and that the overall helix structure is typically B type, also in the modified region (Figure 7).

Analysis of the structure shows that helical parameters throughout the duplex (including the modified part) are indicative of a standard B-type helix as is indicated in Table 3. Backbone angles of the modified region deviate from standard B-type values (Table 3). However, an overlay of a standard thymine deoxyribonucleoside, as it occurs in a standard B-type helix, and the cyclohexenyl-T nucleoside, highlights that the overall structure of both backbones is similar (see Supplementary Material).

## DISCUSSION

As was outlined in the introduction, RNA molecules are characterized by a large functional and structural versatility. Besides forming stable duplexes with other RNA or DNA polymers, RNA has the ability to fold into a large variety of tertiary structures and, in this way, controls a lot of cellular processes (1). This versatility can be partially ascribed to the flexibility of the ribose ring of the RNA building blocks. While ribonucleosides in double-stranded RNA/DNA and RNA/RNA duplexes are predictably structured into a C3′ endo conformation, those which occur in single-stranded regions of the RNA molecule show much more conformational flexibility (51–53). Moreover, it was shown that even in double-stranded regions, the flexibility of oligonucleosides might be necessary to allow recognition of the double-stranded region by enzymes or other cellular structures (54).

While developing chemically modified RNA mimics, research has mainly focused on molecules that show characteristics similar to ribonucleosides that occur in double-stranded RNA regions. Many of these molecules are partially or completely preorganized in a C3′ endo conformation (55). These ‘double-stranded RNA mimics’ are very efficient in forming stable duplexes with RNA and have a prime application in antisense technology. However, to function as real RNA mimics, these molecules are hampered by their structural preorganization. In finding a versatile RNA mimic (not only as a double-stranded molecule but in its complete structural repertoire), development of synthetic nucleosides that show more flexibility is an interesting approach. Constitutionally CeNA can be considered as a DNA mimic (lacking the 2′-OH), conformationally it might behave as an RNA mimic [preference for $_{2}H^{3}$ conformation (N-Type) of the monomer analogs to the puckering mode of the ribose moiety

**Table 3.** Average backbone torsion angles and diagnostic helix parameters in a typical A- and B-type helix and in the modified (CeNA) and unmodified (DNA) part of the duplex

| | A-DNA | B-DNA | CeNA-part | DNA-part |
|---|---|---|---|---|
| α | −50 | −46 | −82.6 (3.2) | −69.7 (3.9) |
| β | 188 | −147 | −196.7 (1.8) | −176.7 (1.7) |
| γ | 41 | 36 | 68.8 (3.5) | 58.3 (4.9) |
| δ | 79 | 157 | 145.1 (3.4) | 140.0 (3.8) |
| ε | −146 | 155 | −151.7 (4.9) | 177.1 (6.9) |
| ζ | −78 | −96 | −121.2 (3.1) | −104.0 (4.2) |
| χ | | | −137 (2.9) | −120 (5.9) |
| Rise | 2.9 | 3.3 | 3.3 (0.2) | 3.2 (0.2) |
| Twist | 31.1 | 36.1 | 38.2 (1.5) | 37.6 (5.2) |
| Inclination | 12.0 | 2.4 | −3.9 (5.3) | 1.1 (6.9) |
| *x*-displacement | 4.10 | 0.8 | −0.2 (0.5) | −0.8 (1.1) |

Averages and standard deviations (between parentheses) were calculated from an ensemble of 25 structures. Torsion angles of the CeNA part are the torsion angles of the incorporated T* nucleotide (Figure 1B). Rise and twist of the CeNA part are an average of the parameters for the base steps GT/AC and TG/AC. Inclination and *x*-displacement of the CeNA part were calculated from their AT* base pair relative to a global helical axis. The backbone is a hybrid of A- and B-DNA; the helical parameters and the ring pucker are more B-DNA like.

in double-stranded RNA]. To evaluate CeNA as conformationally flexible RNA mimic, several studies probing the structure and flexibility of these molecules were performed.

Computational studies on thymidine cyclohexenyl nucleoside and its 2′-ribo-OH and 2′-ara-OH derivatives showed the existence of two low energy states and could shed light on the height of the energy barrier separating the two low energy conformations, which were comparable with the barriers observed in natural ribonucleosides. Furthermore, the results give us some indication of how the conformation and flexibility of the cyclohexenyl nucleosides can be tuned and modulated by choice of the substituents.

The conformation of a cyclohexenyl-U nucleoside was examined by high-resolution NMR spectroscopy. It was shown that the synthetic nucleoside occurs in a high-speed equilibrium between the two states: $_2H^3$ (N-Type) and $^2H_3$ (S-Type), of which the $_2H^3$ conformation is energetically the most favorable. Thermodynamic parameters describing this equilibrium were obtained and show good resemblance with parameters of natural ribonucleosides.

Observing this high degree of equivalence that exists between a cyclohexenyl nucleoside and a ribonucleoside, further studies probing the behavior of cyclohexenyl nucleosides incorporated in duplex structures were started. Ribonucleosides that are incorporated into either RNA or DNA duplexes always seem to show a high tendency to adopt a C3′ endo conformation (52). This behavior, which is quite unexpected given the highly flexible structure of the ribonucleosides, can be mainly explained by the presence of the bulky 2′-OH function, which is also able to form stable hydrogen bonds (either with or without water as a bridging molecule) with other parts of the duplex, when the nucleoside occurs in a C3′ endo conformation. This phenomenon freezes the ribonucleoside in a C3′ endo conformation when incorporated into a duplex structure (52). Cyclohexenyl nucleosides on the other hand do not contain a 2′-OH group, while they do possess a highly flexible structure. Hence, it can be expected that the cyclohexenyl nucleoside should be able to adopt different conformations when incorporated in different kinds of duplexes. In a former study, where a cyclohexenyl adenosine (A*) was incorporated in a self-complementary DNA dodecamer with sequence d(CGCGAA*TTCGCG), a $_2H^3$ conformation (N-Type) of the cyclohexenyl nucleoside was observed and the incorporated nucleoside was found to influence the conformation of neighboring deoxyribonucleosides (9). To investigate whether a cyclohexenyl nucleoside is also able to adopt a $^2H_3$ (S-Type) conformation when incorporated in a DNA duplex, a high-resolution structure of a modified DNA duplex consisting of d(5′-GCGT*GCG-3′) hybridized with d(5′-CGCACGC-3′) was determined using NMR spectroscopy. This sequence was chosen because it allows us to study the behavior of one isolated cyclohexenyl nucleoside in a DNA duplex, whereas the cyclohexenyl nucleoside which was incorporated into the self-complementary Dickerson dodecamer might be influenced by the presence of a cyclohexenyl nucleoside in the opposite strand and/or the sequence context. In contrast to the previously studied sequence, we could now show that the incorporated cyclohexenyl nucleoside occurs in a $^2H_3$ (S-Type) conformation and that the overall helix structure is typically B type, also in the modified region (Figure 7 and Table 3). In this structure, the conformation of the cyclohexenyl nucleotide is influenced by the neighboring deoxynucleotides. This is the first example of a flexible synthetic nucleoside that adopts different conformations when incorporated in different double-stranded DNA sequences. While a free cyclohexene nucleoside exists at 27°C in a fast equilibrium between two low energy states ($_2H^3$ and $_2H^3$ with populations of 56 and 44%, respectively), two cyclohexenyl residues in opposite strands of self-complementary DNA dodecamer adopt the $_2H^3$ (N-type) conformation (9) and the cyclohexenyl residue in the studied heptamer adopts the $^2H_3$ (S-type) conformation which is similar to the conformation of the natural nucleotides in this sequence. This potential for conformational adaptation warrants the evolution of CeNA in biological systems.

It can be argued that cyclohexenyl nucleoside derivatives with a 2′-OH group in ribo position might be more suitable RNA mimics than the unsubstituted cyclohexenyl nucleosides. Indeed, these 'ribo cyclohexenyl nucleosides' were shown to be flexible molecules by computational studies. Furthermore, these molecules possess a 2′-OH group, which might give them properties comparable with natural ribonucleosides. Synthesis of these compounds is currently going on and subsequent structural and functional studies will have to shed light on the properties of these molecules.

## SUPPLEMENTARY MATERIAL

Supplementary Material is available at NAR Online.

## ACKNOWLEDGEMENTS

Authors are indebted to KULeuven (GOA) for financial support. The authors thank P. Gu, G. Schepers and A. Van Aerschot for the synthesis of the CeNA monomer and for oligonucleotides synthesis. K.N. is a Research Assistant of the Fund for Scientific Research, Flanders (Belgium). Funding to pay the Open Access publication charges for this article was provided by KULeuven (GOA grant).

*Conflict of interest statement*. None declared.

## REFERENCES


1. Joyce,G.F. (2002) The antiquity of RNA-based evolution. *Nature*, **418**, 214–221.
2. Anet,F.A.L. (1987) In Rabideau,P.W. (ed.), *The Conformational Analysis of Cyclohexenes, Cyclohexadienes and Related Hydroaromatic Compounds*. VCH Publishers, NY, pp. 1–45.
3. River-Gaines,V.E., Leibowitz,S.J. and Laane,J. (1991) Far-infrared spectra, two-dimensional vibrational potential energy surface, and conformation of cyclohexene and its isotopomers. *J. Am. Chem. Soc.*, **113**, 9735–9742.
4. Anet,F.A.L., Freedberg,D.I., Storer,J.W. and Nouk,K.N. (1992) On the potential energy surface for ring inversion in cyclohexene and related molecules. *J. Am. Chem. Soc*., **114**, 10969–10971.
5. Laane,J. and Choo,J. (1994) The barrier to interconversion of cyclohexene. *J. Am. Chem. Soc*., **116**, 3889–3891.
6. Herdewijn,P. (2001) Cyclohexene nucleic acids: serum stable oligonucleotides that activate RNase H and increase duplex stability with complementary RNA. *Abstr. Pap. Am. Chem. Soc*., **221**, U155.
7. Herdewijn,P. and De Clercq,E. (2001) The cyclohexene ring as bioisostere of a furanose ring: synthesis and antiviral activity of cyclohexenyl nucleosides. *Bioorg. Med. Chem. Lett*., **11**, 1591–1597.
8. Verbeure,B., Lescrinier,E., Wang,J. and Herdewijn,P. (2001) RNase H mediated cleavage of RNA by cyclohexene nucleic acid (CeNA). *Nucleic Acids Res*., **29**, 4941–4947.
9. Wang,J., Verbeure,B., Luyten,I., Lescrinier,E., Froeyen,M., Hendrix,C., Rosemeyer,H., Seela,F., Van Aerschot,A. and Herdewijn,P. (2000) Cyclohexene nucleic acids (CeNA): serum stable oligonucleotides that activate RNase H and increase duplex stability with complementary RNA. *J. Am. Chem. Soc*., **122**, 8595–8602.
10. Wang,J., Verbeure,B., Luyten,I., Froeyen,M., Hendrix,C., Rosemeyer,H., Seela,F., Van Aerschot,A. and Herdewijn,P. (2001) Cyclohexene nucleic acids (CeNA) form stable duplexes with RNA and induce RNase H activity. *Nucleosides Nucleotides Nucleic Acids*, **20**, 785–788.
11. Wang,J., Froeyen,M., Hendrix,C., Andrei,G., Snoeck,R., De Clercq,E. and Herdewijn,P. (2000) The cyclohexene ring system as a furanose mimic: synthesis and antiviral activity of both enantiomers of cyclohexenylguanine. *J. Med. Chem*., **43**, 736–745.
12. Wang,J. and Herdewijn,P. (1999) Enantioselective synthesis and conformational study of cyclohexene carbocyclic nucleosides. *J. Org. Chem*., **64**, 7820–7827.
13. Wang,J. and Herdewijn,P. (1999) Enantioselective synthesis and conformational analysis of cyclohexene carbocyclic nucleosides. *Nucleosides Nucleotides*, **18**, 593–594.
14. Altona,C. and Sundaralingam,M. (1972) Conformational-analysis of sugar ring in nucleosides and nucleotides—new description using concept of pseudorotation. *J. Am. Chem. Soc*., **94**, 8205–8212.
15. Haasnoot,C.A.G. (1992) The conformation of 6-membered rings described by puckering coordinates derived from endocyclic torsion angles. *J. Am. Chem. Soc*., **114**, 882–887.
16. De leeuw,H.P.M., Haasnoot,C.A.G. and Altona,C. (1980) Nucleic-acid constituents .13. Empirical correlations between conformational parameters in beta-D-furanoside fragments derived from a statistical-survey of crystal-structures of nucleic-acid constituents—full description of nucleoside molecular geometries in terms of 4 parameters. *Isr. J. Chem*., **20**, 108–126.
17. Schwieters,C.D., Kuszewski,J.J., Tjandra,N. and Clore,G.M. (2003) The Xplor-NIH NMR molecular structure determination package. *J. Magn. Reson*., **160**, 65–73.
18. Cremer,D. and Szabo,K.J. (1995) In Juaristi,E. (ed.), *Conformational Behavior of Six-Membered Rings*. VHC Publishers, Inc, 114 p.
19. Stewart,J.J.P. (1990) Mopac—a semiempirical molecular-orbital program. *J. Comput. Aid. Mol. Des*., **4**, 1–45.
20. Stewart,J.J.P. (1989) Optimization of parameters for semiempirical methods.1. method. *J. Comput. Chem*., **10**, 209–220.
21. Stewart,J.J.P. (1989) Optimization of parameters for semiempirical methods. 2. applications. *J. Comput. Chem*., **10**, 221–264.
22. Mohamadi,F., Richards,N.G.J., Guida,W.C., Liskamp,R., Lipton,M., Caufield,C., Chang,G., Hendrickson,T. and Still,W.C. (1990) Macromodel—an integrated software system for modeling organic and bioorganic molecules using molecular mechanics. *J. Comput. Chem*., **11**, 440–467.
23. Weiner,S.J., Kollman,P.A., Nguyen,D.T. and Case,D.A. (1986) An all atom force-field for simulations of proteins and nucleic-acids. *J. Comput. Chem*., **7**, 230–252.
24. de Leeuw,F.A.A.M., Vankampen,P.N., Altona,C., Diez,E. and Esteban,A.L. (1984) Relationships between torsion angles and ring-puckering coordinates. 3. Application to heterocyclic puckered 5-membered rings. *J. Mol. Struct*., **125**, 67–88.
25. Altona,C. and Sundaralingam,M. (1973) Conformational-analysis of sugar ring in nucleosides and nucleotides—improved method for interpretation of proton magnetic-resonance coupling-constants. *J. Am. Chem. Soc*., **95**, 2333–2344.
26. Haasnoot,C.A.G., de Leeuw,F.A.A.M. and Altona,C. (1980) The relationship between proton–proton NMR coupling-constants and substituent electronegativities.1. An empirical generalization of the Karplus equation. *Tetrahedron*, **36**, 2783–2792.
27. Friebolin,H. (1991) *Basic One and Two Dimensional NMR Spectroscopy*. VCH, pp. 263–266.
28. de Leeuw,F.A.A.M. and Altona,C. (1982) Conformational-analysis of beta-D-ribo-nucleosides, beta-D-deoxyribo-nucleosides, beta-D-arabino-nucleosides, beta-D-xylo-nucleosides, and beta-D-Lyxo-Nucleosides from proton–proton coupling-constants. *J. Chem. Soc. Perkin Trans*., **2**, 375–384.
29. Haasnoot,C.A.G., de Leeuw,F.A.A.M., De leeuw,H.P.M. and Altona,C. (1981) The relationship between proton–proton NMR coupling-constants and substituent electronegativities. 2. Conformational-analysis of the sugar ring in nucleosides and nucleotides in solution using a generalized Karplus equation. *Org. Magn. Reson*., **15**, 43–52.
30. States,D.J., Haberkorn,R.A. and Ruben,D.J. (1982) A two-dimensional nuclear overhauser experiment with pure absorption phase in 4 quadrants. *J. Magn. Reson*., **48**, 286–292.
31. Plateau,P. and Gueron,M. (1982) Exchangeable proton NMR without base-line distortion, using new strong-pulse sequences. *J. Am. Chem. Soc*., **104**, 7310–7311.
32. Piotto,M., Saudek,V. and Sklenar,V. (1992) Gradient-tailored excitation for single-quantum NMR-spectroscopy of aqueous-solutions. *J. Biomol. NMR*, **2**, 661–665.
33. Rance,M., Sorensen,O.W., Bodenhausen,G., Wagner,G., Ernst,R.R. and Wuthrich,K. (1983) Improved spectral resolution in Cosy H-1-NMR spectra of proteins via double quantum filtering. *Biochem. Biophys. Res. Commun*., **117**, 479–485.
34. Bax,A. and Davis,D.G. (1985) Mlev-17-based two-dimensional homonuclear magnetization transfer spectroscopy. *J. Magn. Reson*., **65**, 355–360.
35. Jeener,J., Meier,B.H., Bachmann,P. and Ernst,R.R. (1979) Investigation of exchange processes by 2-dimensional NMR-spectroscopy. *J. Chem. Phys*., **71**, 4546–4553.
36. Griesinger,C., Otting,G., Wuthrich,K. and Ernst,R.R. (1988) Clean tocsy for H-1 spin system-identification in macromolecules. *J. Am. Chem. Soc*., **110**, 7870–7872.
37. Sklenar,V., Miyashiro,H., Zon,G., Miles,H.T. and Bax,A. (1986) Assignment of the P-31 and H-1 resonances in oligonucleotides by two-dimensional NMR-spectroscopy. *FEBS Lett*., **208**, 94–98.
38. Wijmenga,S.S., Mooren,M.M.W. and Hilbers,C.W. (1993) In Roberts,G.C.K. (ed.), *NMR of Macromolecules: A Practical Approach*, Oxford University Press, Oxford, pp. 217–288.
39. Saenger,W. (1984) *Principles of Nucleic Acid Structure*. Springer Verlag, NY.
40. Wijmenga,S.S. and van Buuren,B.N.M. (1998) The use of NMR methods for conformational studies of nucleic acids. *Prog. Nucl. Magn. Reson. Spectrosc*., **32**, 287–387.
41. Stein,E.G., Rice,L.M. and Brunger,A.T. (1997) Torsion-angle molecular dynamics as a new efficient tool for NMR structure calculation. *J. Magn. Reson*., **124**, 154–164.
42. Lu,X.J., Shakked,Z. and Olson,W.K. (2000) A-form conformational motifs in ligand-bound DNA structures. *J. Mol. Biol*., **300**, 819–840.
43. Kraulis,P.J. (1991) MOLSCRIPT: a program to produce both detailed and schematic plots of protein structures. *J. Appl. Crystallogr*., **24**, 946–950.
44. Esnouf,R.M. (1997) An extensively modified version of molscript that includes generally enhanced colouring capabilities. *J. Mol. Graph. Model*., **15**, 132–134.
45. Levitt,M. and Warshel,A. (1978) Extreme conformational flexibility of furanose ring in DNA and RNA. *J. Am. Chem. Soc*., **100**, 2607–2613.
46. Olson,W.K. (1982) How flexible is the furanose ring. 2. An updated potential-energy estimate. *J. Am. Chem. Soc*., **104**, 278–286.

47. Olson,W.K. and Sussman,J.L. (1982) How flexible is the furanose ring. 1. A comparison of experimental and theoretical-studies. *J. Am. Chem. Soc.*, **104**, 270–278.
48. Thibaudeau,C., Acharya,P. and Chattopadhyaya,J. (1999) *Stereoelectronic Effects in Nucleosides and Nucleotides and Their Structural Implications*. Uppsala University Press, Uppsala.
49. Wütrich,K. (1986) *NMR of Proteins and Nucleic Acids*. Wiley, NY.
50. Delaglio,F., Wu,Z.R. and Bax,A. (2001) Measurement of homonuclear proton couplings from regular 2D COSY spectra. *J. Magn. Reson.*, **149**, 276–281.
51. Lescrinier,E., Froeyen,M. and Herdewijn,P. (2003) Difference in conformational diversity between nucleic acids with a six-membered 'sugar' unit and natural 'furanose' nucleic acids. *Nucleic Acids Res.*, **31**, 2975–2989.
52. Arnott,S. (1999) Polynucleotide secondary structures: an historical perspective. In Neidle,S. (ed.), *Oxford Handbook of Nucleic Acid Structure*. Oxford Press, Oxford, pp. 1–38.
53. Blackburn,G.M. and Gait,M.J. (1996) DNA and RNA structure. In Blackburn,G.M. and Gait,M.J. (eds), *Nucleic Acids in Chemistry and Biology*. Oxford University Press, Oxford, pp. 28–39.
54. Dostal,L., Chen,C.Y., Wang,A.H. and Welfle,H. (2004) Partial B-to-A DNA transition upon minor groove binding of protein Sac7d monitored by Raman spectroscopy. *Biochemistry*, **43**, 9600–9609.
55. Herdewijn,P. (1999) Conformationally restricted carbohydrate-modified nucleic acids and antisense technology. *Biochim. Biophys. Acta*, **1489**, 167–179.